



This is a repository copy of *Analytical prediction of chatter stability for variable pitch and variable helix milling tools*.

White Rose Research Online URL for this paper:
<http://eprints.whiterose.ac.uk/8871/>

Article:

Sims, N.D., Mann, B. and Huyanan, S. (2008) Analytical prediction of chatter stability for variable pitch and variable helix milling tools. *Journal of Sound and Vibration*, 317 (3-5). pp. 664-686. ISSN 0022-460X

<https://doi.org/10.1016/j.jsv.2008.03.045>

Reuse

Unless indicated otherwise, fulltext items are protected by copyright with all rights reserved. The copyright exception in section 29 of the Copyright, Designs and Patents Act 1988 allows the making of a single copy solely for the purpose of non-commercial research or private study within the limits of fair dealing. The publisher or other rights-holder may allow further reproduction and re-use of this version - refer to the White Rose Research Online record for this item. Where records identify the publisher as the copyright holder, users can verify any specific terms of use on the publisher's website.

Takedown

If you consider content in White Rose Research Online to be in breach of UK law, please notify us by emailing eprints@whiterose.ac.uk including the URL of the record and the reason for the withdrawal request.



eprints@whiterose.ac.uk
<https://eprints.whiterose.ac.uk/>

promoting access to White Rose research papers



Universities of Leeds, Sheffield and York
<http://eprints.whiterose.ac.uk/>

This is an author produced version of a paper accepted for publication in **Journal of Sound and Vibration**.

White Rose Research Online URL for this paper:

<http://eprints.whiterose.ac.uk/8871/>

Published paper

Sims, N.D., Mann, B. and Huyanan, S. (2008) *Analytical prediction of chatter stability for variable pitch and variable helix milling tools*. *Journal of Sound and Vibration*, 317 (3-5). pp. 664-686.

<http://dx.doi.org/doi:10.1016/j.jsv.2008.03.045>

Analytical prediction of chatter stability for variable pitch and variable helix milling tools

N D Sims^a, B Mann^b, and S Huyanan^a

^aDepartment of Mechanical Engineering

The University of Sheffield

Mappin St, Sheffield S1 3JD, UK

^b Department of Mechanical Engineering & Materials Science

Duke University

Durham, NC 27708, USA

Abstract

Regenerative chatter is a self-excited vibration that can occur during milling and other machining processes. It leads to a poor surface finish, premature tool wear, and potential damage to the machine or tool. Variable pitch and variable helix milling tools have been previously proposed to avoid the onset of regenerative chatter. Although variable pitch tools have been considered in some detail in previous research, this has generally focussed on behaviour at high radial immersions. In contrast there has been very little work focussed on predicting the stability of variable helix tools. In the present study, three solution processes are proposed for predicting the stability of variable pitch or helix milling tools.

The first is a semi-discretisation formulation that performs spatial and temporal discretisation of the tool. Unlike previously published methods this can predict the stability of variable pitch or variable helix tools, at low or high radial immersions.

The second is a time-averaged semi-discretisation formulation that assumes time-averaged cutting force coefficients. Unlike previous work, this can predict stability of variable helix tools at high radial immersion.

The third is a temporal-finite element formulation that can predict the stability of variable pitch tools with a constant uniform helix angle, at low radial immersion.

The model predictions are compared to previously published work on variable pitch tools, along with time-domain model simulations. Good agreement is found with both previously published results and the time-domain model. Furthermore, cyclic fold bifurcations were found to exist for both variable pitch and variable helix tools at lower radial immersions.

Nomenclature

a	direction coefficient (subscripts x and y denoting two directions)
\bar{a}	average direction coefficient for 1 time step (subscripts x and y denoting directions)
\mathbf{A}	state matrix for the complete system
\mathbf{A}_d	state matrix for the system delays
\mathbf{A}_m	state matrix for the discretised structural dynamics
\mathbf{A}_s	state matrix for the structural dynamics
\mathbf{A}_t	state matrix for the time finite element analysis method
b	depth of cut (m)
\mathbf{B}	input matrix for the complete system
\mathbf{B}_d	input matrix for the system delays
\mathbf{B}_m	input matrix for the discretised structural dynamics
\mathbf{B}_s	input matrix for the structural dynamics
\mathbf{B}_t	delayed state matrix for the time finite element analysis method
\mathbf{C}	output matrix for the complete system
\mathbf{C}_d	output matrix for the system delays
\mathbf{C}_s	output matrix for the structural dynamics
\mathbf{D}	feedthrough matrix for the complete system
\mathbf{D}_d	feedthrough matrix for the system delays
f	force (N) (subscripts n, t, x, y denote normal, tangential, x or y direction)
F	total force (N) (subscripts x, y denote x or y direction)
g	unit step function
h	unit step function
j	index denoting flute (tooth) number
k	index denoting discrete-time step number
K_r	radial relative cutting stiffness (-)
K_t	tangential cutting stiffness (Nm^{-2})
l	index denoting axial layer number
L	number of axial discretisation layers
n	index denoting discrete local time step within a tool revolution
N	number of discrete-time steps per revolution
N_t	Number of flutes (teeth) on the tool
\mathbf{Q}	mapping operator in the time finite element method
\mathbf{R}	state matrix to generate forces based upon state variable Δ
T	sampling time (s)
u	relative vibration (m) (subscripts x, y , denote the x or y direction)
$w_{l,j}$	chip thickness for layer l and flute j (m)
w_0	feed per tooth (m)
\mathbf{x}_d	state variable to determine the delay state Δ
\mathbf{x}_m	state variable for the discretised structural dynamics
\mathbf{x}_s	state variable for the structural dynamics
z	axial position on flute, for the time-finite element method
Δ	state variable defining the difference between current and previous vibrations
Ω	spindle speed (rpm)
α	average direction coefficient for 1 revolution (subscripts x and y denoting directions)
$\phi_{l,j}$	flute angle for layer l and tooth j (rad)
τ	matrix of time delays between flutes

1 Introduction

Despite recent developments in novel manufacturing methods, machining remains one of the most widely used manufacturing processes [1]. The productivity of machining is fundamentally limited by the onset of regenerative chatter [2]. In particular, regenerative chatter can occur when the depth of cut is too large with respect to the dynamic properties of the machine, tool, or workpiece [3]. Regenerative chatter leads to an undesirable surface finish, increased tool wear, and the possibility of damage to the machine itself. Consequently the metal removal rate of the machining process is limited.

As a result, there has been a great deal of research which has aimed to enhance our understanding of the regenerative chatter problem, and to provide methods for enhancing the chatter stability of machining systems. Perhaps the most logical and widely used approach has been to optimise the cutting conditions by determining the so-called stability lobe diagram [3, 4]. With reference to the example in Figure 1, it can be seen that the regenerative chatter stability is a function of depth of cut and spindle speed. Stable cutting can be achieved by increasing the spindle speed which has the additional benefit of increasing the material removal rate (i.e. productivity).

An alternative approach is to increase the damping of the machine, tool, or workpiece, so as to increase the depth of cut at which chatter occurs. Increasing the damping can be achieved by passive [5, 6], semi-active [7-9] or fully active [10-12] means. Another seemingly elegant method is to attempt to break up the mechanism of regenerative chatter by rapidly varying the spindle speed [13, 14]. In practice, however, this requires very high torque from the machine in order to overcome the inertia of the drive system.

For milling problems, the regenerative affect can also be disrupted by changing the pitch and/or helix angle of the tool flutes, as illustrated in Figure 2. For variable pitch tools at high radial immersion, an analytical solution was developed by Altintas *et al* [15]. More recently, this has enabled the optimisation of tool geometry [16]. A novel mathematical approach has also been developed [17] which is well suited to the optimal design of variable pitch tools.

In recent years, the behaviour of milling tools at low radial immersions has been studied in detail. In this configuration, the milling tool is often not engaged in the workpiece. This ‘interrupted cutting’ can lead to different regenerative chatter behaviour that is characterised

by a period doubling or flip bifurcation as opposed to the usual secondary Hopf bifurcation. The stability of interrupted cutting has been studied by Merdol and Altintas [18] (who used a Fourier series expansion of the periodic cutting forces), Insperger *et al* [19, 20] (who used a semi-discretisation approach) and Mann *et al* [21] who used a temporal finite element method). It should be noted that to the authors' knowledge none of this previous work has demonstrated the existence of cyclic fold bifurcations, and it has focussed on regular pitch and regular helix tools.

Furthermore, to the authors' knowledge there has been very little work to predict the stability of variable helix tools in either high or low radial immersions. One exception is the work by Turner *et al* [22]. They proposed that variable helix tools could be modelled by taking the average pitch for each flute, and then applying the variable pitch stability analysis from reference [15]. They showed that the results were acceptable when the axial engagement of the tool was low so that the variable pitch approximation remained valid. They also proposed that differences between experimental results and time-domain simulation results could be attributed to the process damping phenomenon.

The present contribution proposes three model formulations that will be referred to as semi-analytical formulations. The first is a semi-discretisation method, motivated by [19, 20] but suitable for variable pitch/helix tools. The second is a time-averaged semi-discretisation simplification that has similar assumptions to reference [15]. The third is a temporal finite element method based upon reference [23], that is capable of modelling variable pitch tools at low radial immersions with a uniform constant helix angle. Compared to earlier work, the novel contribution of these methods is that they can predict the stability of:

- Variable pitch tools at low radial immersion
- Variable helix tools at low radial immersion
- Variable helix tools at high radial immersion

The remainder of this paper is organised as follows. First, the mechanism of regenerative chatter is described schematically before presenting the three analysis methods. Results for high radial immersion are then compared to previously published work on variable pitch tools. Results at low radial immersion are then compared to previously published work on uniform pitch tools with a constant uniform helix angle. A low radial immersion variable

pitch scenario is then presented, and the results compared to time-domain simulations. Finally, variable helix scenarios are presented for low and high radial immersions, and compared to time-domain simulations.

2 Regenerative chatter

Before presenting the theoretical basis for the proposed modelling methods, it is worthwhile to briefly summarise the mechanism of regenerative chatter, for the sake of completeness. Consider a milling tool (such as that shown in Figure 2), that is up-milling a workpiece. The forces and displacements on a plane normal to tool axis are shown schematically in Figure 3. The forces acting on each tooth can be considered to be a function of the thickness of the chip being removed by that tooth. These forces will cause a relative motion between the tool and the workpiece in the x and y directions. This relative motion imparts a wavy surface finish on the just-cut workpiece, and as the tool rotates this wavy surface is cut by the next tooth. The chip thickness is therefore a function of the current relative displacement and that when the previous tool was cutting the workpiece at this location. The result is a natural feedback process, or self-excited vibration, that can be represented by the schematic block diagram in Figure 4.

In the following sections, models will be developed in order to predict the stability of this self-excited behaviour for variable pitch and/or helix milling tools.

3 Semi-discretisation method

In this method, the semi-discretisation method [19, 20] is adopted, but reformulated with a state-space approach to enable its use on variable pitch and variable helix tools. The methodology can be separated into three aspects: discretisation, cutting force modelling, and state-space formulation. These aspects will now be described.

3.1 Discretisation

Returning to Figure 2, it can be seen that for variable helix tools the delay between each flute varies along the axial depth of the tool. This can be tackled by discretising the tool into L axial layers with depth $\delta b=b/L$, and discretising in the time domain so that N time steps occur in one tool revolution. For consistency with the literature on discrete-time systems [24], the sampling time period is defined as T , and the integer variable $k=1,2,\dots,\infty$ is used to define the value of discrete time, kT . Certain variables are periodic with each tool revolution, which is in

contrast to regular pitch tools that are usually considered periodic with each tooth-pass. The integer variable $n=1,2,\dots,N$ will be used to define the discrete local time nT within each tool revolution.

The relationship between spindle speed Ω (rad/s) and sampling time period T is therefore:

$$T = \frac{2\pi}{N\Omega} \quad (1)$$

As the tool rotates through one complete revolution, the angular position of each axial layer of each flute varies periodically as follows:

$$\phi_{l,j}(nT) = \phi_{l,j}(0T) + \frac{2\pi n}{N} \quad n = 1, 2, \dots, N \quad (2)$$

where $\phi_{l,j}(0T)$ defines the flute geometry of the tool as an angle (in units of radians) from the tool axis to the flute's cutting edge, for each axial discretisation layer l and each flute j .

The pitch between one tooth and the next is given by:

$$\delta\phi_{l,j} = \left\{ \begin{array}{ll} \phi_{l,j+1}(0T) - \phi_{l,j}(0T) & j < N_t \\ \phi_{l,1}(0T) - \phi_{l,j}(0T) + 2\pi & j = N_t \end{array} \right\} \quad j = 1, \dots, N_t \quad (3)$$

where N_t is the number of teeth on the tool. The corresponding time delay between one flute and the next can be described by integer multiples of the sample time T :

$$\tau_{l,j} = T \text{round} \left(N \frac{\delta\phi_{l,j}}{2\pi} \right) \quad (4)$$

where the function *round* represents the rounding of a real number to the nearest integer.

An example is shown in Figure 5. Here, the 16mm diameter tool has two teeth that are 150° and 210° apart at the tool tip. The teeth have helix angles of 50° and 40°. A sample time T is chosen that is $N=60$ times greater than the spindle speed, so that the tool circumference (0 to 360°) can be represented in delay coordinates (0, 1, ..., 60). The fluted region of the tool is divided into five equally sized axial layers of depth $\delta b=0.002\text{m}$. For each slice l of the tool, the delay between one tooth and the next can be obtained by rounding the physical flute position $\phi_{l,j}(0T)$ into an integer delay coordinate. For this example the time delays τ are therefore:

$$\boldsymbol{\tau} = T \begin{bmatrix} 35 & 25 \\ 36 & 24 \\ 37 & 23 \\ 38 & 22 \\ 39 & 21 \end{bmatrix}_{[L \times N_t]} \quad (5)$$

3.2 Cutting force modelling

A discretised axial layer of the milling cutter that is engaged in the workpiece is considered in Figure 3. Assuming a circular tool path and a feed per tooth w_0 , the chip thickness for tooth j on layer l is given by [25-27]:

$$\begin{aligned} w_{l,j} = g(\phi_{l,j}(nT)) & \left[w_0 \sin(\phi_{l,j}(nT)) \right. \\ & + (u_x(kT) - u_x(kT - \tau_{l,j})) \sin(\phi_{l,j}(nT)) \\ & \left. + (u_y(kT) - u_y(kT - \tau_{l,j})) \cos(\phi_{l,j}(nT)) \right] \end{aligned} \quad \begin{array}{l} k = 1, 2, \dots \\ n = 1, 2, \dots, N \end{array} \quad (6)$$

where u_x and u_y are the relative vibrations between the tool and workpiece in the x and y directions respectively. The function g is a unit step function which has value unity when flute j at layer l is engaged in the workpiece:

$$g(\phi_{l,j}(nT)) = \begin{cases} 1 & \leftarrow \phi_{st} < \phi_{l,j}(nT) < \phi_{ex} \\ 0 & \leftarrow \phi_{st} < \phi_{l,j}(nT) \text{ or } \phi_{l,j}(nT) > \phi_{ex} \end{cases} \quad (7)$$

Here, ϕ_{st} and ϕ_{ex} define the angles at which the teeth enter and leave the workpiece. As with previous literature [25] the static component $w_0 \sin(\phi_{l,j})$ in (6) is neglected in the stability analysis because it does not contribute to the regenerative effect. Clearly, the chip generation process depends upon the difference between current relative displacements u_x , u_y , and displacements at previous time points. Unlike uniform pitch tools, however, the time delay τ is not constant for each tooth or axial layer. Consequently, it is useful to define an intermediate state variable Δ that describes the difference between the current discrete-time displacements and the N previous discrete-time displacements within the last revolution:

$$\begin{aligned} \Delta_{x_n}(kT) &= u_x(kT) - u_x(kT - nT) \\ \Delta_{y_n}(kT) &= u_y(kT) - u_y(kT - nT) \end{aligned} \quad (8)$$

The vector $\boldsymbol{\Delta} = \{\boldsymbol{\Delta}_x \quad \boldsymbol{\Delta}_y\}^T$ has size $[2N \times 1]$, and each element describes the vibration relative to a previous sample time in the tool revolution.

Returning to Figure 3, it is commonly assumed [23, 25] that the forces acting on each flute are proportional to the chip thickness, giving:

$$\begin{aligned} f_{t,l,j} &= K_t \cdot \delta b \cdot w_{l,j} \\ f_{n,l,j} &= K_r \cdot f_{t,l,j} \end{aligned} \quad (9)$$

which leads to corresponding forces in the x and y directions:

$$\begin{aligned} f_{x,l,j} &= -f_{t,l,j} \cos(\phi_{l,j}) - f_{n,l,j} \sin(\phi_{l,j}) \\ f_{y,l,j} &= +f_{t,l,j} \sin(\phi_{l,j}) - f_{n,l,j} \cos(\phi_{l,j}) \end{aligned} \quad (10)$$

Substituting (6) and (9) into (10) gives:

$$\begin{aligned} f_{x,l,j} &= \delta b K_t (a_{xx} (u_x(kT) - u_x(kT - \tau_{l,j})) + a_{xy} (u_y(kT) - u_y(kT - \tau_{l,j}))) \\ f_{y,l,j} &= \delta b K_t (a_{yx} (u_x(kT) - u_x(kT - \tau_{l,j})) + a_{yy} (u_y(kT) - u_y(kT - \tau_{l,j}))) \end{aligned} \quad (11)$$

where the instantaneous time varying directional coefficients are:

$$\begin{aligned} a_{xx} &= -g(\phi_{l,j}) [\sin(2\phi_{l,j}) + K_r (1 - \cos(2\phi_{l,j}))] \\ a_{xy} &= -g(\phi_{l,j}) [(1 + \cos(2\phi_{l,j})) + K_r \sin(2\phi_{l,j})] \\ a_{yx} &= +g(\phi_{l,j}) [(1 - \cos(2\phi_{l,j})) - K_r \sin(2\phi_{l,j})] \\ a_{yy} &= +g(\phi_{l,j}) [\sin(2\phi_{l,j}) - K_r (1 + \cos(2\phi_{l,j}))] \end{aligned} \quad (12)$$

The averaged directional coefficients *within* each discretisation time step T can be obtained by integration. In general:

$$\bar{a} = g(\phi) \frac{N}{2\pi} \int_{\phi - \pi/N}^{\phi + \pi/N} a d\phi \quad (13)$$

where the limits of the integration are chosen so that they span an angle $2\pi/N$, which is the angle by which the tool rotates for each discrete-time step. This gives:

$$\begin{aligned} \bar{a}_{xx} &= g(\phi_{l,j}) \frac{N}{4\pi} [\cos 2\phi - 2K_r \phi + K_r \sin 2\phi]_{\phi_{l,j}(nT) - \pi/N}^{\phi_{l,j}(nT) + \pi/N} \\ \bar{a}_{xy} &= g(\phi_{l,j}) \frac{N}{4\pi} [-\sin 2\phi - 2\phi + K_r \cos 2\phi]_{\phi_{l,j}(nT) - \pi/N}^{\phi_{l,j}(nT) + \pi/N} \\ \bar{a}_{yx} &= g(\phi_{l,j}) \frac{N}{4\pi} [-\sin 2\phi + 2\phi + K_r \cos 2\phi]_{\phi_{l,j}(nT) - \pi/N}^{\phi_{l,j}(nT) + \pi/N} \\ \bar{a}_{yy} &= g(\phi_{l,j}) \frac{N}{4\pi} [-\cos 2\phi - 2K_r \phi - K_r \sin 2\phi]_{\phi_{l,j}(nT) - \pi/N}^{\phi_{l,j}(nT) + \pi/N} \end{aligned} \quad (14)$$

Note that these direction coefficients vary periodically with each revolution of the tool. The resulting average forces within each discretisation step are therefore:

$$\begin{aligned}
f_{x,l,j}(kT) &= \delta b K_t (\bar{a}_{xx}(u_x(kT) - u_x(kT - \tau_{l,j})) + \bar{a}_{xy}(u_y(kT) - u_y(kT - \tau_{l,j}))) \\
f_{y,l,j}(kT) &= \delta b K_t (\bar{a}_{yx}(u_x(kT) - u_x(kT - \tau_{l,j})) + \bar{a}_{yy}(u_y(kT) - u_y(kT - \tau_{l,j})))
\end{aligned} \tag{15}$$

These forces can be summed for all teeth and all axial discretisation layers to give the resultant forces, F_x and F_y , in the x and y directions. A corresponding matrix formulation can then be developed by using the variable Δ introduced in (8):

$$\begin{Bmatrix} F_x(kT) \\ F_y(kT) \end{Bmatrix} = \mathbf{R}(nT) \begin{Bmatrix} \Delta_x(kT) \\ \Delta_y(kT) \end{Bmatrix} \tag{16}$$

The elements of the periodic time-varying matrix \mathbf{R} are populated as follows:

$$\begin{aligned}
r_{1,k}(nT) &= \frac{1}{2} \delta b K_t \sum_{j=1}^{N_t} \sum_{l=1}^L h(k, \tau_{l,j}) \bar{a}_{xx}(\phi_{l,j}(nT)) \\
r_{2,k}(nT) &= \frac{1}{2} \delta b K_t \sum_{j=1}^{N_t} \sum_{l=1}^L h(k, \tau_{l,j}) \bar{a}_{xy}(\phi_{l,j}(nT)) \\
r_{1,N+k}(nT) &= \frac{1}{2} \delta b K_t \sum_{j=1}^{N_t} \sum_{l=1}^L h(k, \tau_{l,j}) \bar{a}_{yx}(\phi_{l,j}(nT)) \\
r_{2,N+k}(nT) &= \frac{1}{2} \delta b K_t \sum_{j=1}^{N_t} \sum_{l=1}^L h(k, \tau_{l,j}) \bar{a}_{yy}(\phi_{l,j}(nT))
\end{aligned} \tag{17}$$

where h is a unit step function that defines the appropriate delay term:

$$h(k, \tau_{l,j}) = \begin{cases} 1 & \leftarrow k = \tau_{l,j}/T \\ 0 & \leftarrow k \neq \tau_{l,j}/T \end{cases} \tag{18}$$

3.3 State-space formulation

Returning to Figure 3, the relative motion between the tool and workpiece in the x and y directions have been defined as u_x and u_y , respectively. In the present work these are assumed to be the same for all axial layers of the tool. This relative motion arises due to the structural dynamics of the tool or workpiece, which can be represented in state-space form as:

$$\begin{aligned}
\{\dot{\mathbf{x}}_s\}_{[D \times 1]} &= \mathbf{A}_s \mathbf{x}_s + \mathbf{B}_s \begin{Bmatrix} F_x \\ F_y \end{Bmatrix} \\
\begin{Bmatrix} u_x \\ u_y \end{Bmatrix}_{[2 \times 1]} &= \mathbf{C}_s \mathbf{x}_s
\end{aligned} \tag{19}$$

where the subscript s denotes the structural dynamics, and D is the total number of states used to model the vibration in the x and y directions.

Discretising the continuous time dynamics (19) gives:

$$\begin{aligned}\mathbf{x}_m(kT + T) &= \mathbf{A}_m \mathbf{x}_m(kT) + \mathbf{B}_m \begin{Bmatrix} F_x(kT) \\ F_y(kT) \end{Bmatrix} \\ \begin{Bmatrix} u_x(kT) \\ u_y(kT) \end{Bmatrix} &= \mathbf{C}_s \mathbf{x}_m(kT)\end{aligned}\quad (20)$$

where \mathbf{A}_m and \mathbf{B}_m are given by the matrix exponential:

$$\begin{bmatrix} [\mathbf{A}_m]_{[D \times D]} & [\mathbf{B}_m]_{[D \times 2]} \\ - & - \end{bmatrix}_{[(D+2) \times (D+2)]} = \exp\left(T \begin{bmatrix} [\mathbf{A}_s]_{[D \times D]} & [\mathbf{B}_s]_{[2 \times D]} \\ [\mathbf{0}]_{[2 \times D]} & [\mathbf{0}]_{[2 \times 2]} \end{bmatrix}\right)\quad (21)$$

Meanwhile, the relationship between the relative vibration \mathbf{u} and the delay state Δ can be represented in discrete-time state-space form as:

$$\begin{aligned}\mathbf{x}_d(kT + T) &= \mathbf{A}_d \mathbf{x}_d(kT) + \mathbf{B}_d \begin{Bmatrix} u_x(kT) \\ u_y(kT) \end{Bmatrix} \\ \begin{Bmatrix} \Delta_x(kT) \\ \Delta_y(kT) \end{Bmatrix} &= \mathbf{C}_d \mathbf{x}_d(kT) + \mathbf{D}_d \begin{Bmatrix} u_x(kT) \\ u_y(kT) \end{Bmatrix}\end{aligned}\quad (22)$$

The terms in (22) are:

$$\begin{aligned}\mathbf{A}_d &= \begin{bmatrix} \begin{bmatrix} \{0 \ \cdots \ 0\}_{[N-1]} & 0 \\ [I]_{[(N-1) \times (N-1)]} & \{0 \ \cdots \ 0\}_{[N-1]}^T \end{bmatrix} & [0] \\ [0] & \begin{bmatrix} \{0 \ \cdots \ 0\}_{[N-1]} & 0 \\ [I]_{[(N-1) \times (N-1)]} & \{0 \ \cdots \ 0\}_{[N-1]}^T \end{bmatrix} \end{bmatrix} \\ \mathbf{B}_d &= \begin{bmatrix} \{1 \ \{0 \ \cdots \ 0\}_{[N-1]}^T\} & \{0 \ \cdots \ 0\}_{[N-1]}^T \\ \{0 \ \cdots \ 0\}_{[N]}^T & \{1 \ \{0 \ \cdots \ 0\}_{[N-1]}^T\} \end{bmatrix} \\ \mathbf{C}_d &= \begin{bmatrix} -[\mathbf{I}]_{[N \times N]} & [0] \\ [0] & -[\mathbf{I}]_{[N \times N]} \end{bmatrix} \\ \mathbf{D}_d &= \begin{bmatrix} \{1 \ \cdots \ 1\}_{[N]}^T & \{0 \ \cdots \ 0\}_{[N]}^T \\ \{0 \ \cdots \ 0\}_{[N]}^T & \{1 \ \cdots \ 1\}_{[N]}^T \end{bmatrix}\end{aligned}\quad (23)$$

The schematic block diagram shown in Figure 4 can now be replaced by the mathematical model shown in Figure 6. Combining (20), (22) and (16) gives:

$$\begin{Bmatrix} \mathbf{x}_m(kT + T) \\ \mathbf{x}_d(kT + T) \end{Bmatrix} = \mathbf{A} \begin{Bmatrix} \mathbf{x}_m(kT) \\ \mathbf{x}_d(kT) \end{Bmatrix} + \mathbf{BC}(nT) \begin{Bmatrix} \mathbf{x}_m(kT) \\ \mathbf{x}_d(kT) \end{Bmatrix}\quad (24)$$

where:

$$\begin{aligned}
\mathbf{A} &= \begin{bmatrix} \mathbf{A}_m & [\mathbf{0}] \\ \mathbf{B}_d \mathbf{C}_s & \mathbf{A}_d \end{bmatrix} \\
\mathbf{B} &= \begin{bmatrix} \mathbf{B}_m \\ [\mathbf{0}]_{[2N \times 2]} \end{bmatrix} \\
\mathbf{C}(nT) &= [\mathbf{R}(nT) \mathbf{D}_d \mathbf{C}_s \quad \mathbf{R}(nT) \mathbf{C}_s]
\end{aligned} \tag{25}$$

Consequently the states of the system vary between one tool revolution and the next tool revolution as follows:

$$\begin{Bmatrix} \mathbf{x}_m(kT + NT) \\ \mathbf{x}_d(kT + NT) \end{Bmatrix} = (\mathbf{A} + \mathbf{BC}(NT))(\mathbf{A} + \mathbf{BC}((N-1)T))(\dots)(\mathbf{A} + \mathbf{BC}(T)) \begin{Bmatrix} \mathbf{x}_m(kT) \\ \mathbf{x}_d(kT) \end{Bmatrix} \tag{26}$$

The asymptotic stability of the system is therefore governed by the eigenvalues or characteristic multipliers of $(\mathbf{A} + \mathbf{BC}(NT))(\mathbf{A} + \mathbf{BC}((N-1)T))(\dots)(\mathbf{A} + \mathbf{BC}(T))$. Characteristic multipliers (CM's) with magnitude greater than unity indicate an asymptotically unstable system, i.e. chatter, and the value of the maximum CM as it crosses the unit circle indicates the type of bifurcation which occurs [28]. For a secondary Hopf or Neimark bifurcation, the maximum CM crosses the unit circle with a non-zero imaginary component, and quasi-periodic motion occurs. For a period doubling or flip bifurcation, the maximum CM crosses the unit circle at -1, and period two motion occurs. For a saddle-node or cyclic fold bifurcation, the maximum CM crosses the unit circle at +1, and period one motion occurs. Cyclic fold bifurcations are often associated with the 'jump phenomenon' where the periodic motion is replaced by another remote solution as the control parameter (i.e. depth of cut) is increased [28]. To the authors' knowledge, cyclic fold bifurcations have not been observed in previous work on milling chatter, except where it arises due to tool runout [29]. However, it should be noted that Insperger and Stepan [30] identified similar behaviour during turning operations with a periodically varying spindle speed.

4 Time averaged semi-discretisation approach

In this section, the semi-discretisation method will now be simplified slightly. A considerable amount of computation time is required to compute the product $(\mathbf{A} + \mathbf{BC}(NT))(\mathbf{A} + \mathbf{BC}((N-1)T))(\dots)(\mathbf{A} + \mathbf{BC}(T))$ in Eq. (26) when the order N is large. This issue can be avoided if the time varying direction coefficients are averaged across an entire tool revolution. In general:

$$\alpha = g(\phi) \frac{N}{2\pi} \int_0^{2\pi} a d\phi = \frac{N}{2\pi} \int_{\phi_{st}}^{\phi_{ex}} a d\phi \quad (27)$$

This is equivalent to the assumption used by Budak and Altintas [31] who expressed the direction coefficients as a Fourier series and selected only the first term in the series. The resulting time-averaged direction coefficients are:

$$\begin{aligned} \alpha_{xx} &= \frac{1}{4\pi} [\cos 2\phi - 2K_r \phi + K_r \sin 2\phi]_{\phi_{st}}^{\phi_{ex}} \\ \alpha_{xy} &= \frac{1}{4\pi} [-\sin 2\phi - 2\phi + K_r \cos 2\phi]_{\phi_{st}}^{\phi_{ex}} \\ \alpha_{yx} &= \frac{1}{4\pi} [-\sin 2\phi + 2\phi + K_r \cos 2\phi]_{\phi_{st}}^{\phi_{ex}} \\ \alpha_{yy} &= \frac{1}{4\pi} [-\cos 2\phi - 2K_r \phi - K_r \sin 2\phi]_{\phi_{st}}^{\phi_{ex}} \end{aligned} \quad (28)$$

It should be noted that these differ from the values given by Altintas [25] by a factor of N , because in the present formulation the summation for all teeth occurs separately. Since these coefficients are no longer periodically time varying, Eq. (16) can be rewritten with a constant value for \mathbf{R} :

$$\begin{Bmatrix} F_x(kT) \\ F_y(kT) \end{Bmatrix} = \mathbf{R} \begin{Bmatrix} \Delta_x(kT) \\ \Delta_y(kT) \end{Bmatrix} \quad (29)$$

Where the constant elements of \mathbf{R} are:

$$\begin{aligned} r_{1,k} &= \frac{1}{2} \delta b K_t \sum_{j=1}^{N_t} \sum_{l=1}^L h(k, \tau_{l,j}) \alpha_{xx} \\ r_{2,k} &= \frac{1}{2} \delta b K_t \sum_{j=1}^{N_t} \sum_{l=1}^L h(k, \tau_{l,j}) \alpha_{xy} \\ r_{1,N+k} &= \frac{1}{2} \delta b K_t \sum_{j=1}^{N_t} \sum_{l=1}^L h(k, \tau_{l,j}) \alpha_{yx} \\ r_{2,N+k} &= \frac{1}{2} \delta b K_t \sum_{j=1}^{N_t} \sum_{l=1}^L h(k, \tau_{l,j}) \alpha_{yy} \end{aligned} \quad (30)$$

The state-space representation of the system is now given by:

$$\begin{Bmatrix} \mathbf{x}_m(kT+T) \\ \mathbf{x}_d(kT+T) \end{Bmatrix} = \mathbf{A} \begin{Bmatrix} \mathbf{x}_m(kT) \\ \mathbf{x}_d(kT) \end{Bmatrix} + \mathbf{BC} \begin{Bmatrix} \mathbf{x}_m(kT) \\ \mathbf{x}_d(kT) \end{Bmatrix} \quad n = 1, 2, \dots, N \quad (31)$$

where:

$$\begin{aligned}
\mathbf{A} &= \begin{bmatrix} \mathbf{A}_m & [\mathbf{0}] \\ \mathbf{B}_d \mathbf{C}_s & \mathbf{A}_d \end{bmatrix} \\
\mathbf{B} &= \begin{bmatrix} \mathbf{B}_m \\ [\mathbf{0}]_{[2N \times 2]} \end{bmatrix} \\
\mathbf{C} &= [\mathbf{R} \mathbf{D}_d \mathbf{C}_s \quad \mathbf{C}_s]
\end{aligned} \tag{32}$$

Consequently, stability can be determined directly from the eigenvalues of $(\mathbf{A}+\mathbf{BC})$.

The advantages of this time-averaged semi-discretisation formulation are twofold. First, the computation time is faster as previously mentioned. Second, the formulation is equivalent to the method of Altintas and Budak [31] in that the direction coefficients are time-averaged in the same fashion. This allows the axial and temporal discretisation methodology to be validated by a direct comparison with published work on variable pitch tools.

5 Time Finite Element Formulation

A key issue with the previous two methods is that they perform axial discretisation of the tool, as well as discretisation in the time domain. Although the convergence of time domain semi-discretisation was investigated by reference [19], axial discretisation has not previously been considered for semi-analytical models. It is therefore important to compare the stability predictions with those from alternative models that do not perform axial discretisation of the tool. Recent work by Patel, Mann, and Young [23] has investigated the stability of uniform pitch tools at low radial immersions, and shown that the constant helix angle of the tool has a significant effect on the period doubling bifurcation behaviour. This method performed analytical integration over the axial length of the tool, and the approach will now be extended to consider the case of a variable pitch tool, under the assumption that only one flute is engaged in the workpiece at any one point in time. For the sake of brevity, a full derivation is not presented here. Instead, the theory described by [23] is briefly outlined, with emphasis on modification of the approach for the case of variable pitch tools. It should be noted that this will enable the constant helix angle of a variable pitch tool to be considered, but the approach is not yet suitable for variable helix angle tools.

Patel *et al* [23] considered a single-degree of freedom vibration aligned with the tool feed direction (i.e. the x -direction of Figure 3). They showed that the cutting force in the x -direction can be written as a continuous function of the axial position z and time delay τ as:

$$F_x = \int_{z_1(t)}^{z_2(t)} -g(z,t) \left(\frac{w_0 + u_x(t) - u_x(t-\tau)}{2} \right) [K_t \sin 2\theta + K_t K_r (1 - \cos 2\theta)] dz \quad (33)$$

The limits of integration were shown to be piecewise continuous and can be summarised graphically with the help of Figure 7. In the first regime (Figure 7a) a flute is entering the cut, whilst in the second regime (Figure 7b) a flute is in the middle of the cut (and may or may not be engaged in the workpiece across its entire length). In the third regime (Figure 7c) the tool leaves the cut, and this is followed by a period of time where there are no cutting forces and the tool experiences a free vibrational decay (Figure 7d). This process is then repeated for the next flute on the tool (Figure 7e).

For a uniform pitch tool, the solution to the equation of motion is periodic for each flute (Figure 7a to d). Whilst an analytical solution for the free decay behaviour (Figure 7d) is straightforward, the behaviour during cutting is described by a delay-differential equation which is solved with an approximation method. Patel [23] and previous authors [29] have applied the temporal finite element analysis (TFEA) method, which allows the delay-differential equation to be transformed into a discrete map.

To implement the TFEA method, the delay-differential equation is first written in state-space form as:

$$\dot{\mathbf{y}}(t) = \mathbf{A}_t(t)\mathbf{y}(t) + \mathbf{B}_t(t)\mathbf{y}(t-\tau) \quad (34)$$

Where \mathbf{A}_t is the state matrix and \mathbf{B}_t is the delayed state matrix. An assumed solution is used for the states \mathbf{y} and the delayed states $\mathbf{y}(t-\tau)$. The method of weighted residuals is then applied to the assumed solution, so as to minimise its error [32]. The results from each temporal element can then be combined, along with the equation describing the free-decay behaviour, to form a discrete map in the form:

$$\mathbf{y}_j = \mathbf{Q}\mathbf{y}_{j-1} \quad j = 1, 2, \dots \quad (35)$$

which describes the states of the system for each tooth pass j as a function of the states for the previous tooth pass $j-1$.

It transpires that this procedure can be readily extended to the problem of variable pitch tools provided that only one tool is in contact with the workpiece at any one point in time. The method of Patel *et al* [23] is simply applied to each flute of the tool in turn. The matrix \mathbf{Q} will be different for each flute because each flute will have its own delay term τ in (34).

Consequently, Eq. (34) and (35) must be rewritten for each flute, leading to the behaviour from one *tool revolution* to the next:

$$\mathbf{y}_j = \mathbf{Q}_{N_t} \mathbf{Q}_{N_t-1} \cdots \mathbf{Q}_1 \mathbf{y}_{j-N_t} \quad (36)$$

The stability of the system can therefore be determined by the eigenvalues or characteristic multipliers of the product $\mathbf{Q}_{N_t} \mathbf{Q}_{N_t-1} \cdots \mathbf{Q}_1$.

6 Results: uniform and variable pitch tools

So far, two modelling approaches have been proposed for predicting the stability of variable helix tools, and one method for predicting stability for variable pitch tools with a constant uniform helix angle, at low radial immersion. The predictions from these models will now be compared to previously published results and time-domain simulations.

6.1 High radial immersion

To illustrate the performance of the approach on standard and variable pitch milling tools, the work of Budak, Engin and Altintas [15] is reconsidered. In [15] and [17], a milling tool was investigated under the conditions described in Table 1. Analytical solutions were developed for the uniform pitch and variable pitch tools, and (for the variable pitch tool) these were compared to substantial experimental data as well as time-domain model results. It was demonstrated that the analytical method provided very accurate prediction of the chatter stability. In Figure 8 the results using the time-averaged semi-discretisation approach are compared to Altintas's analytical method, using the same parameters as their experimental work [17]. It can be seen that the time-averaged semi-discretisation approach agrees closely with the results of prior work.

For the uniform pitch tool, Altintas's analytical result does not require an iterative method and so the result can be computed very quickly – 0.2 seconds on a 1.7GHz laptop. Meanwhile, the time-averaged semi-discretisation solution took 30 seconds. The difference between the two approaches can be attributed to the convergence issues when using the time-averaged semi-discretisation approach, along with the effect of the interpolation or contouring between the data points.

For the variable pitch tool, Altintas's method requires an iterative approach to search for an admissible real-valued eigenvalue for each data-point on the curve. Consequently the solution

time is much slower and depends to a large extent on the efficiency of the programming code. For the code used in the present study the solution was obtained in 70 seconds. In contrast, the time-averaged semi-discretisation approach still took 30 seconds, since the problem formulation is essentially the same as for a uniform pitch tool. Furthermore, the time-averaged semi-discretisation approach allows the user to specify the spindle speed at which the results are computed. In contrast, Altintas's variable pitch solution gives this information as an output, and as a result the data points on Figure 8b are not regularly spaced.

This agreement between the proposed time-averaged semi-discretisation model and the work of others serves to validate the time-averaged semi-discretisation approach for a variable pitch problem at high radial immersion.

6.2 Lower radial immersions

At lower radial immersions, a semi-discretisation approach is more appropriate than the fully discrete method since it is able to capture the period-doubling, or flip bifurcations, that give rise to periodic loss of contact for different flutes of the tool. Recent work [23] has demonstrated experimentally the stability of uniform pitch tools at low radial immersions, with special emphasis on the role of a constant uniform helix angle on the stability boundary. The cutting scenario considered in reference [23] is summarized in Table 2, and in the present contribution this work is extended to consider the variable pitch tool (also described in Table 2).

For the uniform pitch tool the original TFEA solution [23] is compared to the time-averaged semi-discretisation and semi-discretisation methods in Figure 9a. It can be seen that the semi-discretisation method agrees closely with the TFEA method, and is able to predict the so-called 'islands of instability' that were obtained in reference [23]. This is a useful result since the semi-discretisation predictions required axial discretisation of the tool, and yet they agree closely with an experimentally validated model that did not require axial discretisation. It should be noted that these islands of instability arising due to period doubling bifurcations were first observed by Zatarain *et al* [33].

It can be seen from Figure 9a that the time-averaged semi-discretisation method gives stability boundaries that resemble those from the TFEA and semi-discretisation methods, but

that the prediction cannot model the islands of instability. This is due to the time-averaged cutting force model which is not able to predict the onset of period-doubling bifurcations.

For completeness, the prediction from the semi-discretisation method is compared to Patel and Mann's experimental data [23] in Figure 9b. This experimental data focussed on the island of instability, and it can be seen that the predicted stability boundary agrees closely with the experimental data.

For a variable pitch tool the new TFEA solution is compared to the time-averaged semi-discretisation and semi-discretisation methods in Figure 10a. Again, the semi-discretisation and TFEA solutions agree closely, whilst the time-averaged semi-discretisation method fails to predict the period-doubling bifurcations.

The behaviour shown in Figure 10a has not yet been compared to experimental data. Consequently, the variable pitch scenario was also compared to a time-domain simulation. This simulation used the model described in reference [34], which is a kinematic model of the milling process based upon reference [35] but implemented in Simulink. The model was configured to use 20 axial discretisations of the tool, 500 simulated tool revolutions, and 2048 time steps per revolution, and the convergence of the solution was verified. Once per revolution samples of the simulated vibration were plotted to explore the stability of the simulated response, along with recordings of the chip thickness. The simulation was repeated for 32 different spindle speeds and 31 different depths of cut between 0.5mm and 16mm.

The results from the time-domain simulation are compared to the semi-analytical methods in Figure 10b. It can be seen that the time domain model agrees very closely with the proposed semi-analytical methods. Of particular interest, however, is the behaviour in the regions indicated as 'A' and 'B' on Figure 10b. This behaviour is explored in detail in Figure 11, which shows the eigenvalues (Characteristic Multipliers) obtained using the semi-discretisation method, along with the 1/revolution samples from the time-domain simulation. The 1/revolution samples were obtained by performing a separate simulation at each depth of cut, and plotting the 1/revolution displacement for the last 10 cycles of the tool. If the simulated response is stable then these last 10 cycles should have reached a steady-state forced-vibration condition, which means that they should all have the same 1/revolution sampled value, and should appear as a discrete point on the diagram. In Figure 11b, this can be seen to occur for depths of cut up to 6mm. Beyond this point, period two motion can be

seen to occur: the 1/rev samples alternate between two values indicating a period doubling or flip bifurcation. This bifurcation is accurately predicted by the semi-discretisation method: the characteristic multipliers (Figure 11a) cross the unit circle at -1 when the depth of cut increases from 6 to 7mm. As the depth of cut is increased further, the time-domain simulation shows a secondary Hopf bifurcation at 12mm.

Figure 11c and d correspond to case 'B' on Figure 10. In this case, the semi-discretisation characteristic multipliers indicate a cyclic-fold bifurcation between 4mm and 5mm. This is particularly interesting since to the authors' knowledge there have been no previous reports (analytical or experimental) of this particular behaviour during milling. It is however acknowledged that cyclic fold bifurcations can occur if tool runout is considered, and that similar bifurcation behaviour has been observed for variable speed turning operations [30].

The existence of a cyclic fold bifurcation cannot be directly shown from the bifurcation diagram shown in Figure 11d, since the post-bifurcation behaviour still exhibits period one motion. However, Figure 11d shows a secondary Hopf bifurcation at 14mm, and at this bifurcation there is a sharp discontinuity in the value of the 1/rev samples, which is indicative of the 'jump phenomena' associated with cyclic fold bifurcations [28].

In Figure 12 the behaviour for cases 'A' and 'B' are further explored by plotting the simulated chip thickness for the final two simulated tool revolutions. The tooth number of each of the three teeth is labelled to help illustrate the periodicity of the solution. For case 'A' (Figure 12a) at 5.5mm depth cut, the simulated response is stable and periodic with each tool revolution. At 7.5mm depth cut, the response is periodic over two tool revolutions and one of the flutes has lost contact with the workpiece on alternate revolutions. This clearly indicates a period-doubling bifurcation. For case 'B' (Figure 12b) at 2mm depth cut, the response is stable and periodic with each tool revolution. However, when the depth of cut is increased to 3mm, one of the flutes loses contact with the workpiece during the cut (Tooth 1 at samples 400 to 440, and 2450 to 2490). This behaviour repeats itself *every* tool revolution. Consequently the loss-of-contact is associated with a cyclic fold bifurcation, rather than a period doubling bifurcation.

Returning to Figure 10b, this loss-of-contact behaviour can be seen superimposed on the stability predictions. It can now be seen that the cyclic-fold bifurcation that is predicted by the TFEA and semi-discretisation methods is associated with a period-one loss-of-contact in the

time domain simulation. Further work is needed to explore this issue in detail, but based upon the findings here, an interesting corollary emerges: Period doubling bifurcations are associated with a flute of the tool failing to engage in the workpiece during alternating revolutions [29], whilst the cyclic fold bifurcation appears to be associated with a lack of engagement for *every* revolution.

To summarise the results so far, the fully discrete method has been shown to match experimentally validated work on uniform and variable pitch tools at high radial immersion. Meanwhile, the semi-discretisation method matches experimentally validated work on uniform pitch tools with a constant uniform helix angle at low radial immersion. The method also agrees closely with the proposed variable pitch TFEA method, as well as a comprehensive time domain simulation.

In the next section, the time-averaged semi-discretisation and semi-discretisation methods will be compared to time domain simulations for variable helix tools.

7 Results: Variable helix tools

As for the earlier results, a single-degree-of-freedom flexure was considered and the tool itself assumed to be rigid. Two cutting scenarios were considered: a three-flute variable pitch tool with a 1mm radial immersion down-milling cut, and a two flute variable pitch tool with a full immersion cut. The details are shown in Table 2. Comprehensive time-domain simulations were performed over an appropriate range of spindle speeds and depths of cut. As before, 1/revolution sampling was performed to determine the existence of period doubling or secondary Hopf bifurcations, and the simulated chip thickness was examined to determine any stable loss-of-contact.

The results for the three-flute tool at low radial immersion are shown in Figure 13. The semi-discretisation approach indicates a region of instability that is governed by secondary Hopf bifurcations which has a different shape to that of the classical stability lobes for a regular tool (Figure 1). The unstable region is also in contrast to the islands of instability observed by Patel [23] and Zatarain [33] which are associated with period doubling bifurcations rather than secondary Hopf bifurcations. The time-averaged semi-discretisation prediction agrees reasonably closely with the semi-discretisation prediction, but can only predict the existence of secondary Hopf bifurcations. The corresponding time-domain simulation results are shown in Figure 13b. The secondary Hopf and period doubling bifurcations agree closely with those

from the semi-analytical methods, but there are more scenarios where a cyclic fold bifurcation occurs. As mentioned earlier, further work is needed to properly characterise this stable loss-of-contact behaviour.

The results for the two-flute tool at full radial immersion are shown in Figure 14. In this case, only secondary Hopf bifurcations were observed in the semi-analytical methods and also in the time-domain simulation. The semi-discretisation predictions agree closely with the time-domain simulation, but the time-averaged semi-discretisation method does not predict the same stability boundary. For this example, the region of instability around 1400rpm, 2mm is clearly an isolated island of instability due to secondary Hopf bifurcations. Again, this is in contrast to the period doubling islands of instability described by Patel [23] and Zatarain [33].

8 Discussion

The new theoretical formulations have shown strong agreement with previously published work as well as with time-domain simulations. However, various aspects of the results are worthy of further discussion.

First, from a practical aspect, the stability of variable pitch / helix tools could be strongly influenced by issues such as milling tool run-out or eccentricity, and nonlinearity in the relationship between cutting force and chip thickness. Furthermore, the as-manufactured tool geometry (pitch and helix angles) may differ from that used for the stability prediction. However, predictions investigated by the authors to date have suggested that the stability boundaries for variable pitch and variable helix tools tend to change smoothly as the tool geometry is modified. Although the models have been shown to compare well with previous experimental data on variable pitch tools (at high radial immersion), and regular helix tools (at low radial immersions), it is clear that more experimental testing is needed. This is particularly true for the case of variable helix tools, where the models have only been validated against time-domain simulations. This will be the subject of future work.

From a process design aspect, the stability of variable helix tools has been shown to exhibit some interesting and unusual behaviour that could be of interest to the machinist. In particular, it has been shown that such tools can re-stabilise at higher depths of cut, suggesting that greater productivity can be achieved. However, this behaviour is strongly related to the structural dynamics of the system, suggesting that the tools are most likely to be of use for very specific applications, rather than general machining. Meanwhile, variable pitch tools

have been shown to suffer from additional unstable behaviour as their radial immersion is reduced. Unfortunately this period-one instability seems to coincide with the increased stability that was achieved by introducing the variable pitch geometry. For example, in Figure 9 at around 2500 rpm the stable depth is about 4mm, and for the equivalent variable pitch tool (Figure 10) this is increased to 8mm, *except* for the region of period-one instability. This suggests that great care must be exercised when using variable pitch tools at a low radial immersion.

From a nonlinear dynamics aspect, more work is needed to explore the behaviour associated with the cyclic fold bifurcation in variable pitch tools. However, numerical or experimental investigation of cyclic fold bifurcation would require a simulation or experiment whose parameters (depth of cut and spindle speed) could be slowly varied during the (simulated) cut run so as to obtain a bifurcation diagram. This would be a challenging exercise for both physical experiments and numerical simulations.

Finally, it is interesting to note that the time-averaged semi-discretisation method was reasonably accurate for the variable pitch tool at low radial immersions, but less accurate for the full radial immersion case. This result is counter-intuitive since it would be expected that the time-averaged cutting force coefficients were a better approximation as the cut became less interrupted (i.e. at higher radial immersion). One possible explanation is as follows. The existence of islands of secondary Hopf bifurcation instability, such as that shown in Figure 14, show that the stability of the tool can both increase and decrease as the depth of cut is increased. Consequently there can be regions where the stability of the tool has a local minima, without actually becoming unstable. In these regions, the error due to the use of time-averaged cutting force coefficients may cause the local minima to be unstable.

9 Conclusions

This work has proposed three alternative model formulations for regenerative chatter in milling. Unlike previously published work, the models are between them able to predict the stability of:

- Variable pitch tools at low radial immersion,
- Variable helix tools at low radial immersion,
- Variable helix tools at high radial immersion.

Although new experimental data has not been presented, good agreement was found with previously published work [15] on variable pitch tools at high radial immersion. Good agreement was also found with previously published work [23] that considered the constant uniform helix angle of a uniform pitch tool. Furthermore, all the models were compared against a comprehensive set of time-domain simulations. However, experimental work is needed to investigate the effect of issues such as run-out, and sensitivity to the as-manufactured tool geometry.

Of the three models presented, the TFEA method was the most efficient numerically, but its application is currently limited to variable pitch tools at low radial immersion. The semi-discretisation method was applicable to all types of tools, but was numerically intensive. The time-averaged semi-discretisation method was faster to compute, but the approximations in the cutting force coefficient led to greater deviation compared to time-domain or previous experimental data.

The stability predictions have indicated that at low radial immersions variable pitch tools suffer from an additional region of instability that may reduce the advantage gained by introducing the pitch variation. Meanwhile, variable helix tools exhibit islands of instability, suggesting that large productivity improvements could be possible by increasing the axial depth of cut. However, this behaviour is dependant upon the tool geometry and structural dynamics of the system. Consequently the tools may only be useful for specific machining problems.

For a variable pitch and helix tools at low radial immersion, previously unreported cyclic-fold bifurcations were predicted. In the time-domain model this bifurcation was found to be associated with tooth loss-of-contact that repeated periodically with every revolution of the tool. This is in contrast to the behaviour observed in a period-doubling bifurcation, where tooth loss-of-contact occurs periodically with every two revolutions of the tool. However, the loss-of-contact behaviour was found to be more widespread in the time-domain simulation results than for the predictions from the semi-discretisation method.

Acknowledgements.

NDS is grateful for the support of the EPSRC (GR/S49841/01 and GR/S49858/01).

References

- [1] J. Tlustý, *Manufacturing process and equipment*, 1st edition ed: Prentice-Hall, 2000.
- [2] M. Wiercigroch and E. Budak, "Sources of nonlinearities, chatter generation and suppression in metal cutting," *Philosophical Transactions of the Royal Society of London, Part A*, vol. 359, pp. 663-693, 2001.
- [3] J. Tlustý, "Dynamics of High-Speed Milling," *Journal of Engineering for Industry*, vol. 108, pp. 59-67, 1986.
- [4] Y. Altintas and E. Budak, "Analytical prediction of stability lobes in milling," *CIRP Annals*, vol. 44, pp. 357-362, 1995.
- [5] Y. S. Tarn, J. Y. Kao, and E. C. Lee, "Chatter suppression in turning operations with a tuned vibration absorber," *Journal of Materials Processing Technology*, vol. 105, pp. 55-60, 2000.
- [6] N. D. Sims, A. Amarasinghe, and K. Ridgway, "Particle dampers for workpiece chatter mitigation," presented at 2005 ASME International Mechanical Engineering Congress and Exposition, November 5-11, 2005, Orlando, Florida USA, 2005.
- [7] D. J. Segalman and J. M. Redmond, "Chatter suppression through variable impedance and smart fluids," *Proceedings of SPIE - The International Society for Optical Engineering*, v 2721, (1996), p 353-363.
- [8] M. Wang and R. Fei, "Chatter suppression based on nonlinear vibration characteristic of electrorheological fluids," *International Journal of Machine Tools and Manufacture*, vol. 39, pp. 1925-1934, 1999.
- [9] M. Wang and R. Fei, "Improvement of machining stability using a tunable-stiffness boring bar containing an electrorheological fluid," *Smart Materials and Structures*, pp. 511-514, 1999.
- [10] J. L. Dohner, J. P. Lauffer, T. D. Hinnerichs, N. Shankar, M. Regelbrugge, C.-M. Kwan, R. Xu, B. Winterbauer, and K. Bridger, "Mitigation of chatter instabilities in milling by active structural control," *Journal of Sound and Vibration*, vol. 269, pp. 197-211, 2004.
- [11] N. D. Sims and Y. Zhang, "Piezoelectric Active Control for Workpiece Chatter Reduction during Milling," presented at Smart Structures and Materials 2004: Smart structures and integrated systems, 2004.
- [12] J. R. Pratt and A. H. Nayfeh, "Chatter control and stability analysis of a cantilever boring bar under regenerative cutting conditions," *Philosophical Transactions of the Royal Society of London, Part A*, vol. 359, pp. 759-792, 2001.
- [13] E. Al-Regib, J. Ni, and S.-H. Lee, "Programming spindle speed variation for machine tool chatter suppression," *International Journal of Machine Tools and Manufacture*, vol. 43, pp. 1229-1240, 2003.
- [14] Y. Altintas and P. K. Chan, "In-process detection and suppression of chatter in milling," *International Journal of Machine Tools and Manufacture*, vol. 32, pp. 329-347, 1992.
- [15] Y. Altintas, S. Engin, and E. Budak, "Analytical prediction of chatter stability and design for variable pitch cutters," *Journal of Manufacturing Science and Engineering*, vol. 121, pp. 173-178, 1999.
- [16] E. Budak, "An analytical design method for milling cutter with nonconstant pitch to increase stability, part 2: application," *Journal of Manufacturing Science and Engineering*, vol. 125, pp. 35-38, 2003.
- [17] N. Olgac and R. Sipahi, "A unique methodology for chatter stability mapping in simultaneous machining," *Journal of Manufacturing Science and Engineering*, vol. 127, pp. 791-800, 2005.
- [18] S. D. Merdol and Y. Altintas, "Multi frequency solution of chatter stability for low immersion milling," *Journal of Manufacturing Science and Engineering, Transactions of the ASME*, vol. 126, pp. 459-466, 2004.
- [19] F. Hartung, T. Insperger, G. Stepan, and J. Turi, "Approximate stability charts for milling processes using semi-discretization," *Applied Mathematics And Computation*, vol. 174, pp. 51-73, 2006.
- [20] T. Insperger and G. Stepan, "Updated semi-discretization method for periodic delay-differential equations with discrete delay," *International Journal for Numerical Methods in Engineering*, vol. 61, pp. 117, 2004.
- [21] B. P. Mann, P. V. Bayly, M. A. Davies, and J. E. Halley, "Limit cycles, bifurcations, and accuracy of the milling process," *Journal Of Sound And Vibration*, vol. 277, pp. 31-48, 2004.
- [22] S. Turner, D. Merdol, Y. Altintas, and K. Ridgway, "Modelling of the stability of variable helix end mills," *International Journal of Machine Tools and Manufacture*, vol. 47, pp. 1410, 2007.

- [23] B. R. Patel, B. P. Mann, and K. A. Young, "Uncharted islands of chatter instability in milling," *International Journal of Machine Tools & Manufacture*, vol. 48, pp. 124-134, 2008.
- [24] Ogata, *Discrete time control systems*. New Jersey: Prentice Hall, 1995.
- [25] Y. Altintas, *Manufacturing Automation: Metal Cutting Mechanics, Machine Tool Vibrations, and CNC Design*: Cambridge University Press, 2000.
- [26] M. E. Martellotti, "An analysis of the milling process," *Transactions of ASME*, vol. 63, pp. 677-700, 1941.
- [27] M. E. Martellotti, "An analysis of the milling process. part ii: down milling," *Transactions of ASME*, vol. 67, pp. 233-251, 1945.
- [28] L. N. Virgin, *Introduction to experimental nonlinear dynamics: a case study in mechanical vibration*. Cambridge: Cambridge University Press, 2000.
- [29] B. P. Mann, K. A. Young, T. L. Schmitz, and D. D. Dilley, "Simultaneous stability and surface location error in milling," *Journal of Manufacturing Science and Engineering*, vol. 127, pp. 446-453, 2005.
- [30] T. Insperger and G. Stefan, "Stability analysis of turning with periodic spindle speed modulation via semidiscretization," *JVC/Journal of Vibration and Control*, vol. 10, pp. 1835, 2004.
- [31] E. Budak and Y. Altintas, "Analytical prediction of chatter stability in milling - part II: application of the general formulation to common milling systems," *Journal of Dynamic Systems, Measurement and Control*, vol. 120, pp. 31-36, 1998.
- [32] J. N. Reddy, *An Introduction to the Finite Element Method*, 2nd ed. New York: McGraw-Hill, 1993.
- [33] M. Zatarain, J. Munoa, G. Peigne, and T. Insperger, "Analysis of the influence of mill helix angle on chatter stability," *CIRP Annals - Manufacturing Technology*, vol. 55, pp. 365, 2006.
- [34] N. Sims, "The self-excitation damping ratio: a chatter criterion for time-domain milling simulations," *Journal of Manufacturing Science and Engineering*, vol. 127, pp. 433-445, 2005.
- [35] M. L. Campomanes and Y. Altintas, "An improved time domain simulation for dynamic milling at small radial immersions," *Journal of Manufacturing Science and Engineering*, vol. 125, pp. 416-422, 2003.

Tool diameter (mm)	19.05		
Number of flutes	4		
Variable flute pitch	70°-110°-70°-110°		
Uniform flute pitch	90°-90°-90°-90°		
Helix angle	30°		
Radial immersion (mm)	9.525		
Milling mode	Down milling		
K_t (MPa)	697		
K_r (-)	0.367		
x-direction modes			
Natural frequencies (Hz)	441.64	563.6	778.56
Modal effective masses (kg)	11.125	1.4986	13.063
Damping ratios (-)	0.028722	0.055801	0.058996
y-direction mode			
Natural frequency (Hz)	516.21		
Modal effective mass (kg)	1.199		
Damping ratio (-)	0.025004		

Table 1: Tool and cutting parameters for the uniform tool and variable pitch tool studies.

	Flute pitch	Flute Helix
Uniform pitch tool	120°-120°-120°	30°-30°-30°
Variable pitch tool	120°-100°-140°	30°-30°-30°
Variable helix tool 1	120°-100°-140°	25°-30°-35°
Variable helix tool 2	180°-180°	30°-55°
Tool diameter (mm)	19.05	
Radial immersion (mm)	1.00 (19.05 for Variable helix tool 2)	
K_t (MPa)	550	
K_r (-)	0.3636	
x-direction mode		
Natural frequency (Hz)	169.3	
Modal effective mass (kg)	6.5363	
Damping ratio (-)	0.0056	

Table 2: Tool and cutting parameters for the flexure studies.

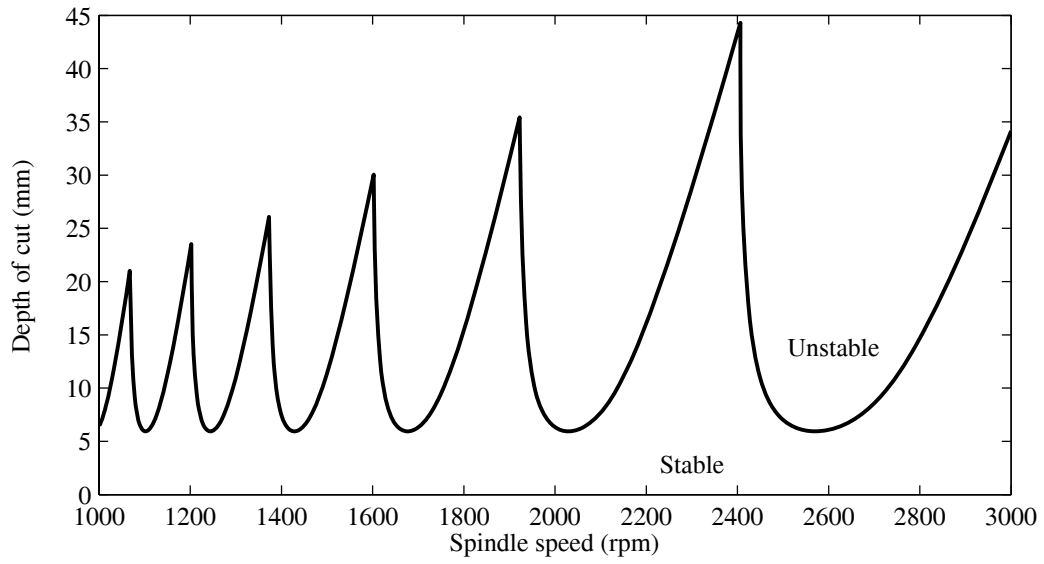


Figure 1: Typical stability lobe diagram depicting the relationship between spindle speed, depth of cut, and chatter.

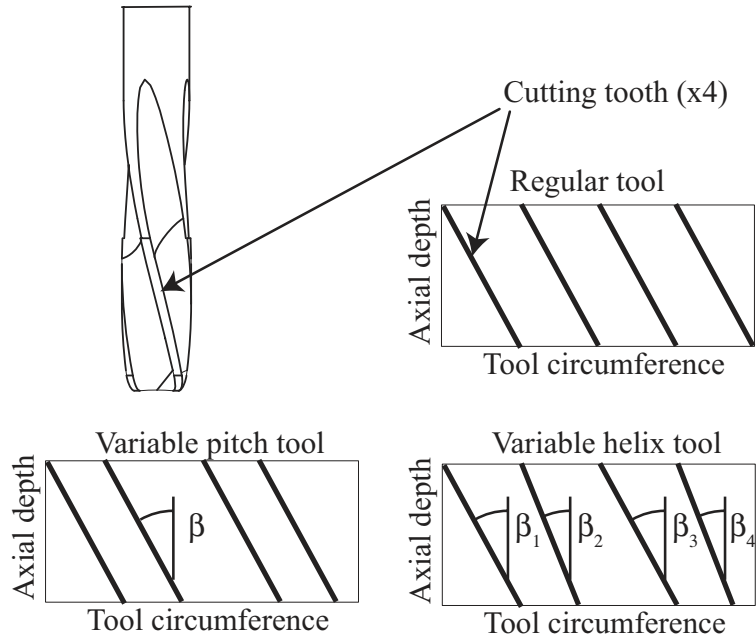


Figure 2: Uniform, variable pitch, and variable helix tools.

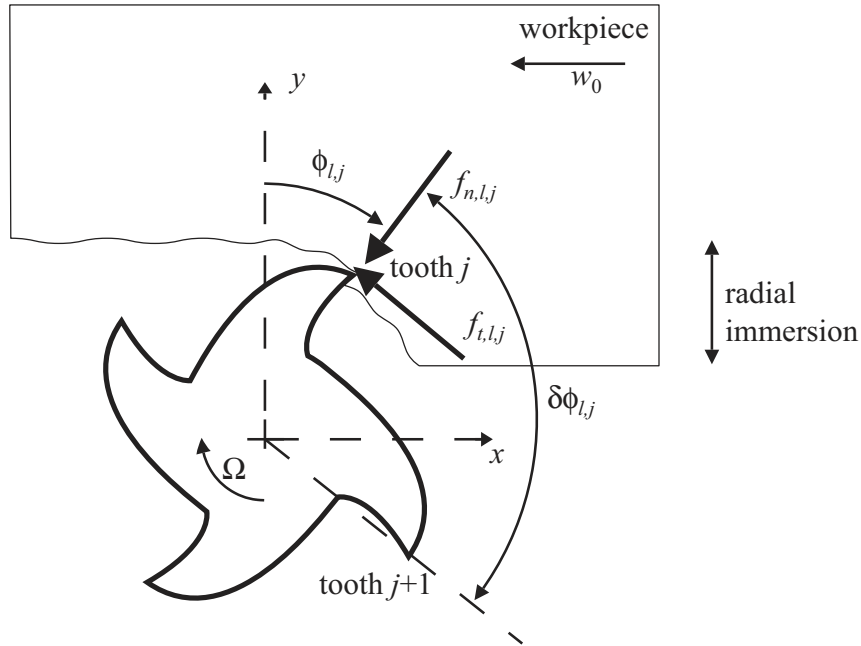


Figure 3: Forces on axial slice l of a tool (up milling).

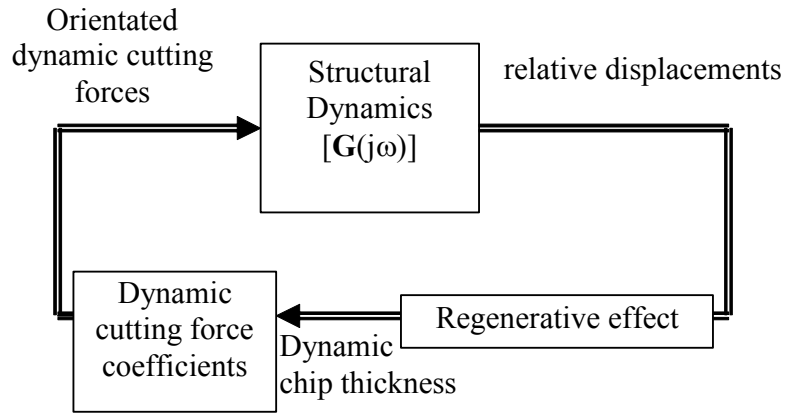


Figure 4: Schematic block diagram for regenerative chatter in milling.

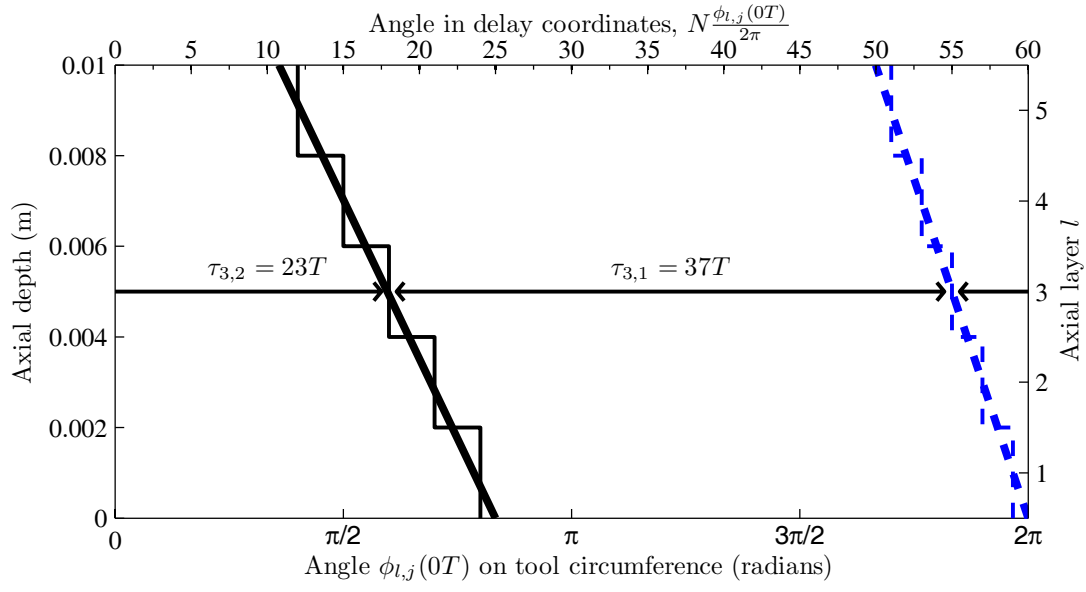


Figure 5: Discretisation of the time delays for a variable helix tool.
— tooth $j=1$; **—** tooth $j=1$ (discretised); **— — —** tooth $j=2$; **- - -** tooth $j=2$ (discretised).

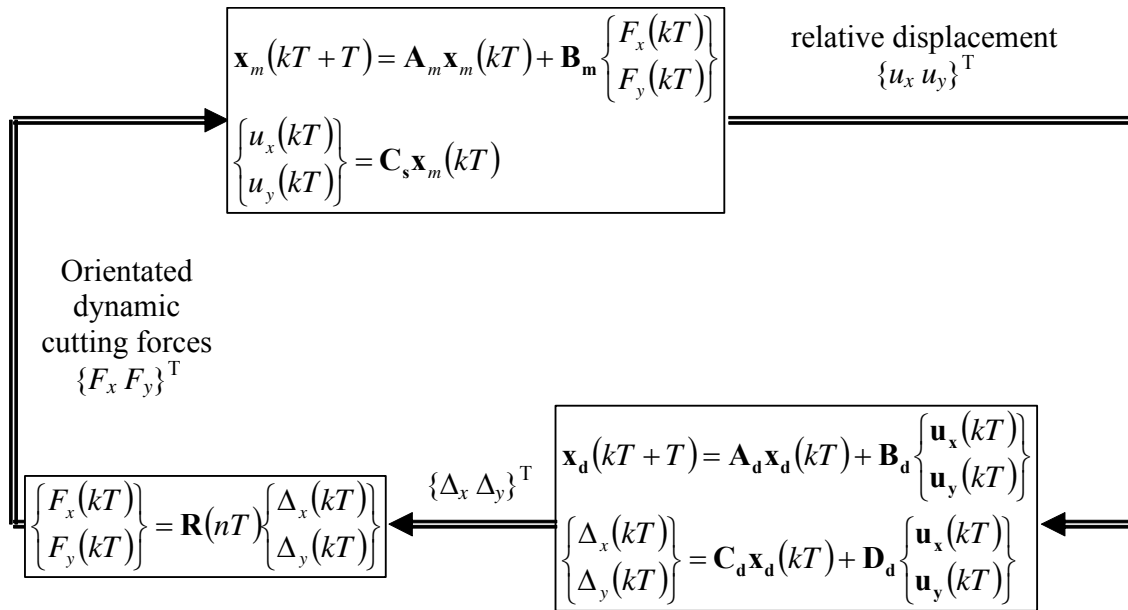


Figure 6: Block diagram in state-space form

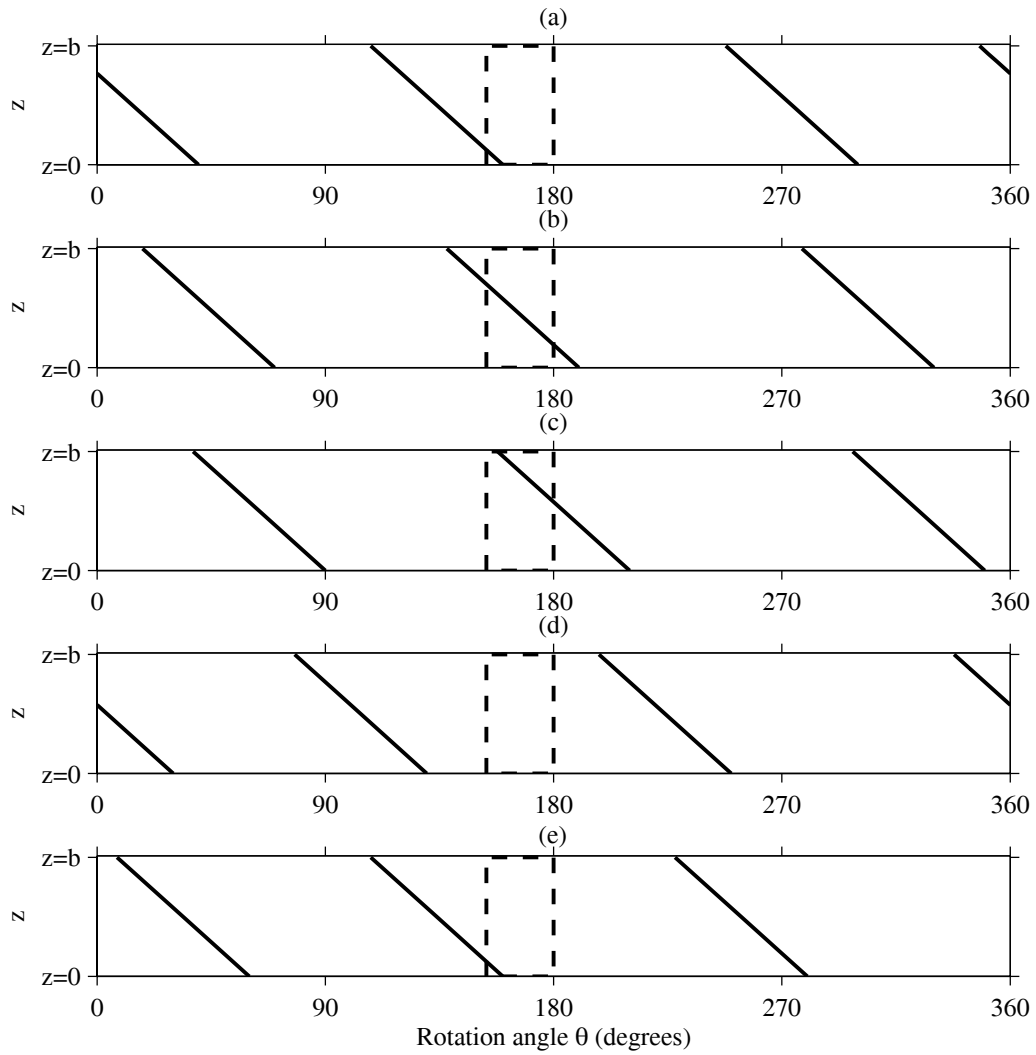


Figure 7: Cutting force regimes for the TFEA model. The dashed line represents the angular region where the tool is engaged in the workpiece for a downmilling operation. (a) Flute 1 entry; (b) Flute 1 middle; (c) Flute 1 exit; (d) Free decay; (e) Flute 2 entry.

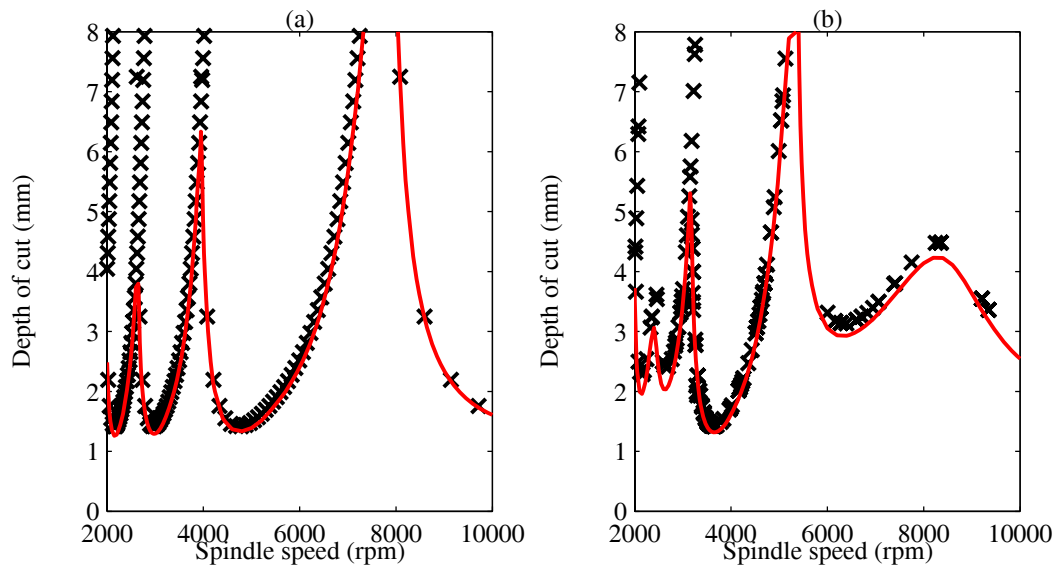


Figure 8: Comparison of stability predictions.
 — time-averaged semi-discretisation method; × method of Altintas [15].
 (a) Uniform pitch tool; (b) Variable pitch tool.

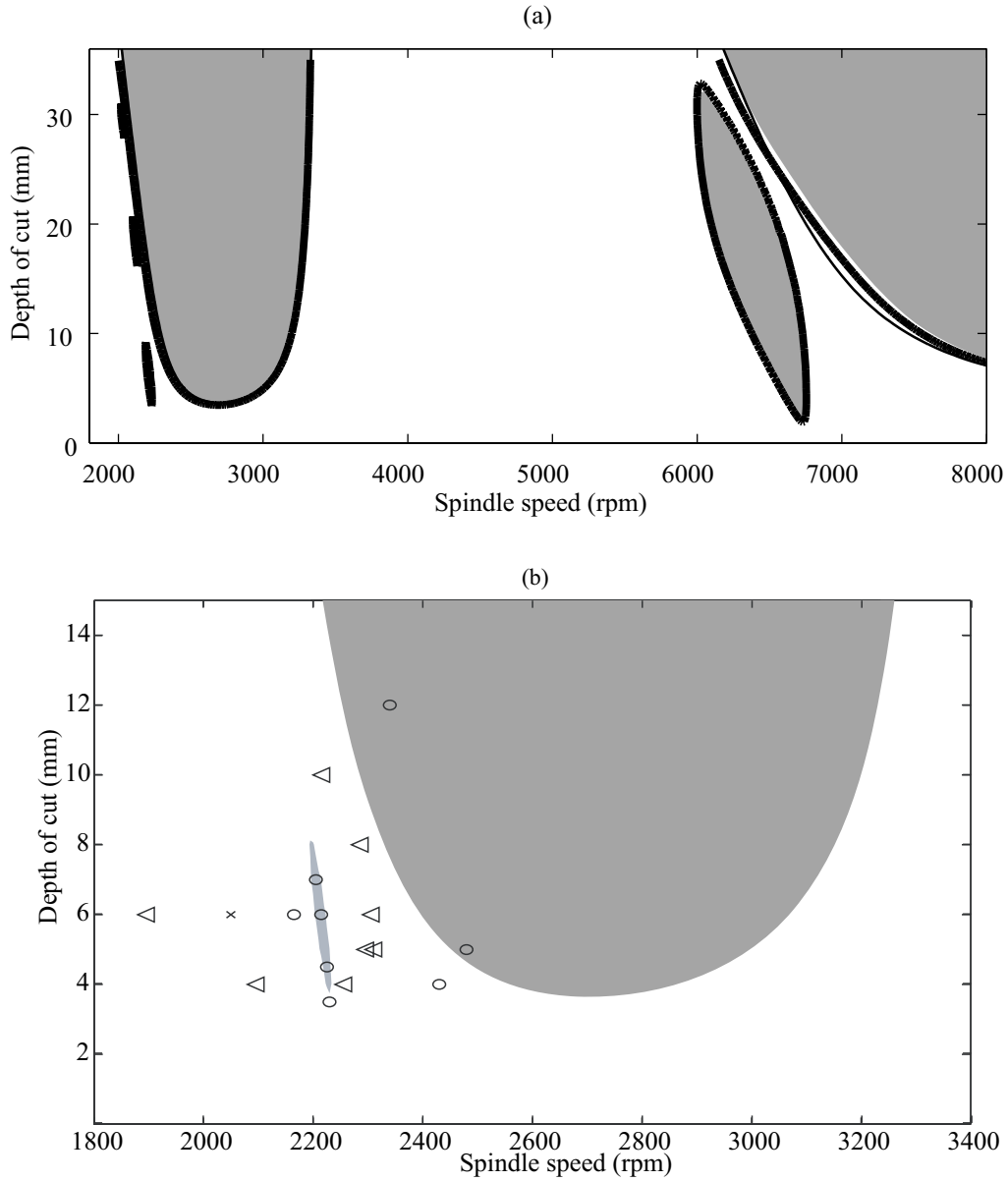


Figure 9: Stability lobes for the single-degree of freedom flexure considered by Patel and Mann [23].

(a) New model formulations

(b) Comparison of the time-averaged semi-discretisation method with the experimental data in [23].

■ semi-discretisation method

— time-averaged semi-discretisation method

— TFEA method.

◁ stable experimental tests; ○ unstable tests; × tests that were not clearly stable or unstable.

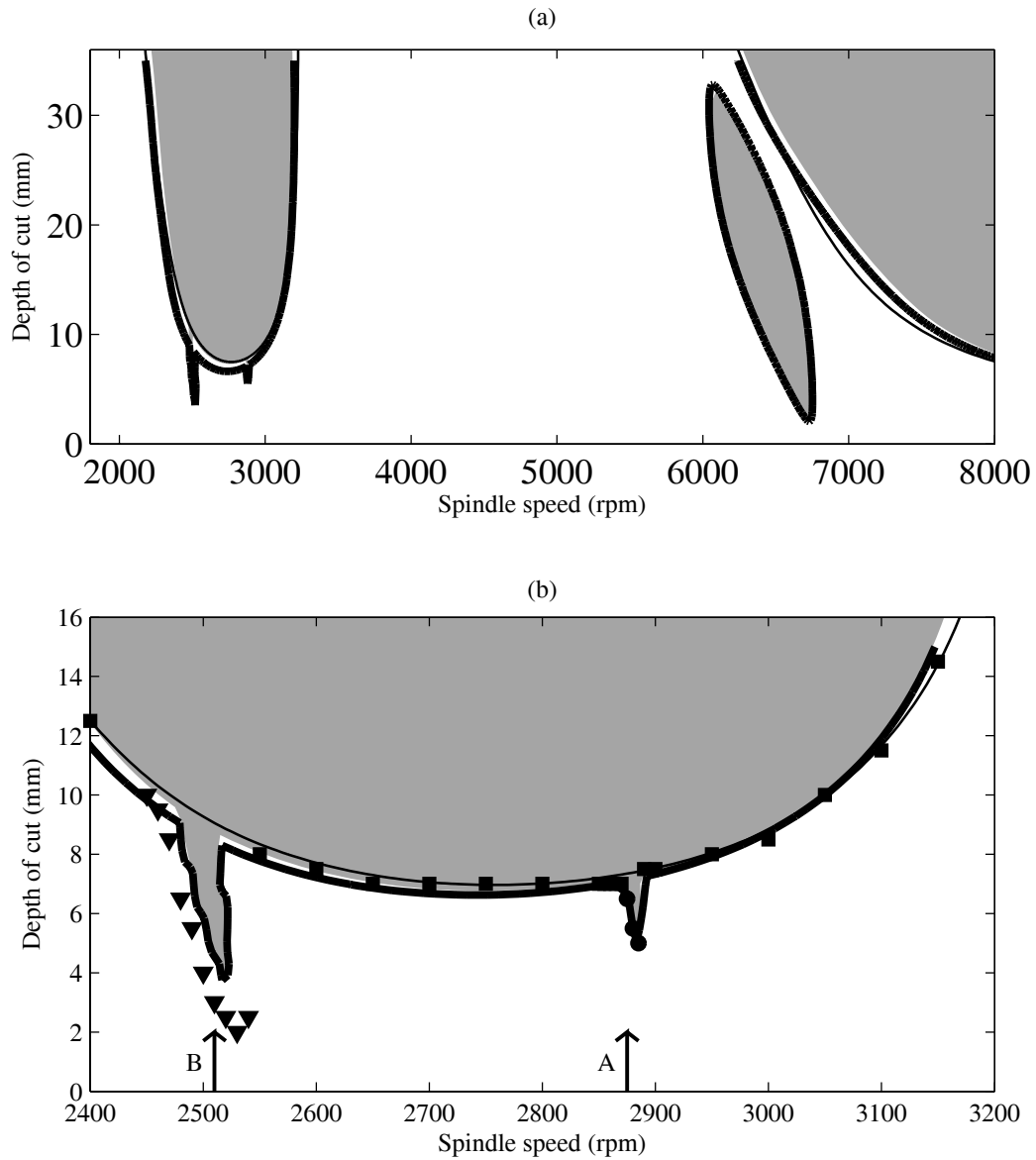


Figure 10: Stability predictions for a variable pitch (120-100-140) tool.

(a) Semi-analytical methods

(b) Comparison with time-domain simulations.

■ semi-discretisation method

— time-averaged semi-discretisation method

— TFEA method.

The solid markers represent time-domain simulation results, and indicate the lowest depth of cut that showed a particular behaviour at each spindle speed. ■ secondary Hopf bifurcation; ▼ cyclic fold bifurcation; • period doubling bifurcation.

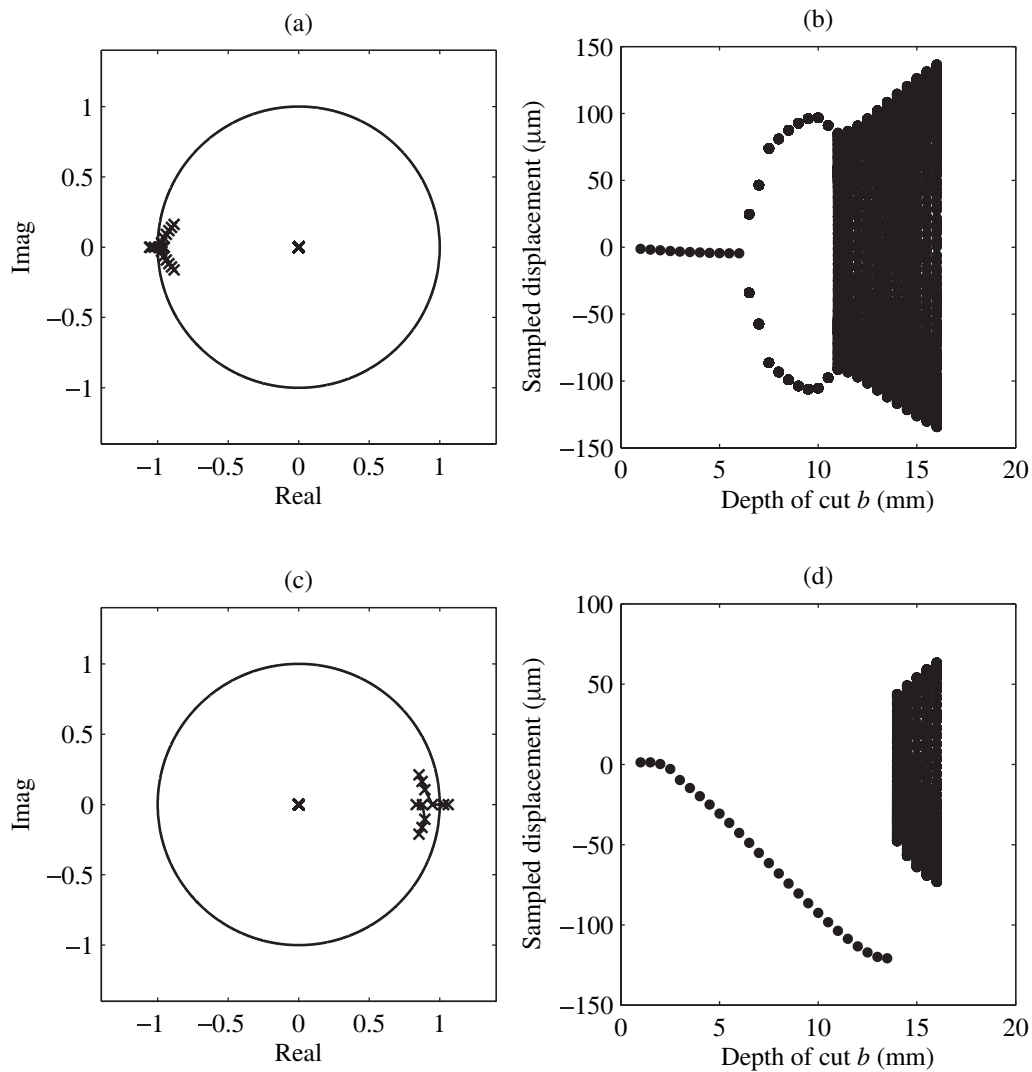


Figure 11: Stability analysis for the semi-discretisation and time-domain methods.
(a) Characteristic multipliers at 2875rpm (case 'A'), $b=1,2,\dots,9$ mm (b) 1/rev samples of steady-state vibration at 2875rpm.
(c) Characteristic multipliers at 2510rpm (case 'B'), $b=1,2,\dots,6$ mm (d) 1/rev samples of steady-state vibration at 2510rpm.

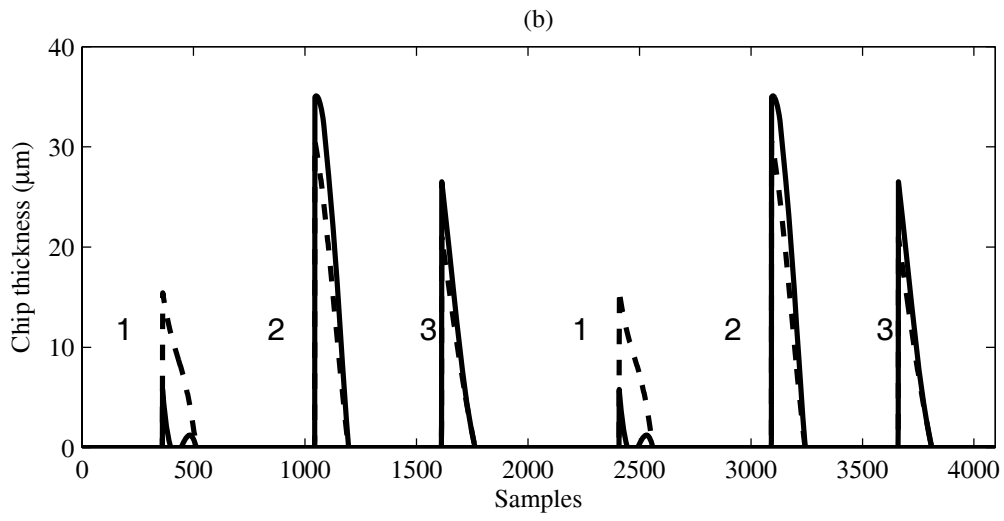
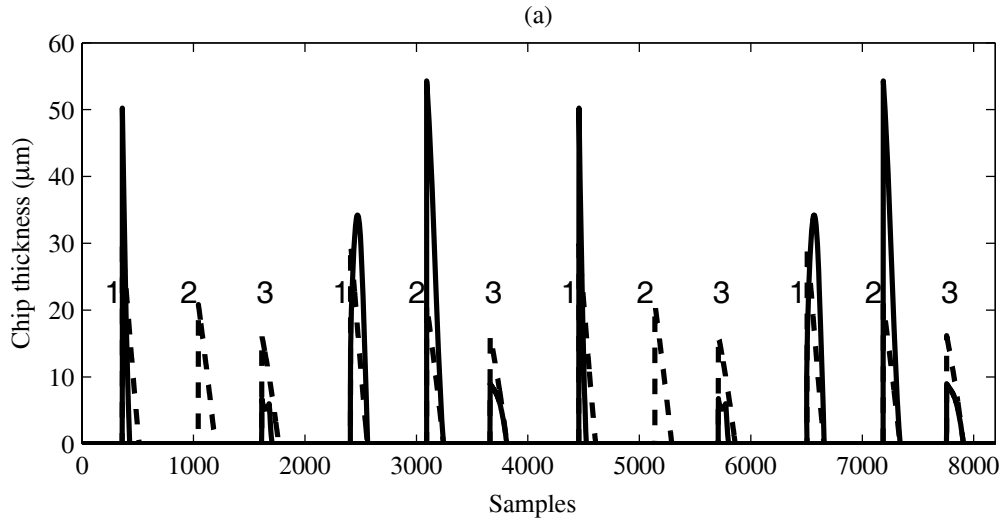


Figure 12: Chip thickness prediction (for one axial slice of the tool) from the time-domain simulation. The ‘flute number’ is shown for each tooth to indicate the periodicity of the solution
(a) 2875 rpm (case ‘A’). - - - $b=5.5\text{mm}$; — $b=7.5\text{mm}$.
(b) 2510 rpm (case ‘B’). - - - $b=2\text{mm}$; — $b=3\text{mm}$.

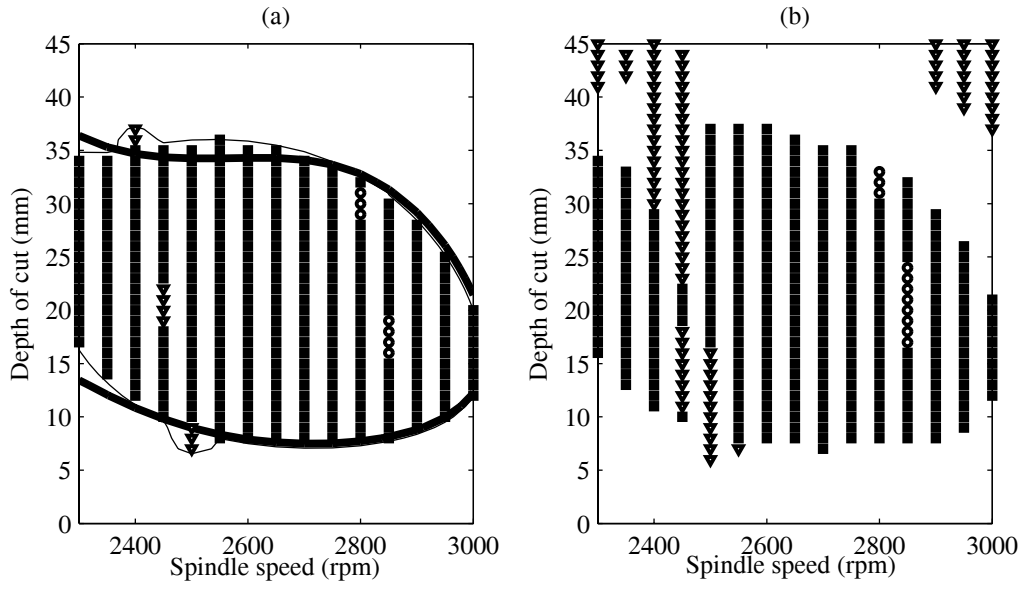


Figure 13: Stability predictions for a three-flute variable helix tool at 5.25% radial immersion.
(a) semi-analytical methods (b) time domain simulation.
— time-averaged semi-discretisation method;
— and markers: semi-discretisation method
■ secondary Hopf bifurcation; ○ period doubling bifurcation; ▽ cyclic fold bifurcation.

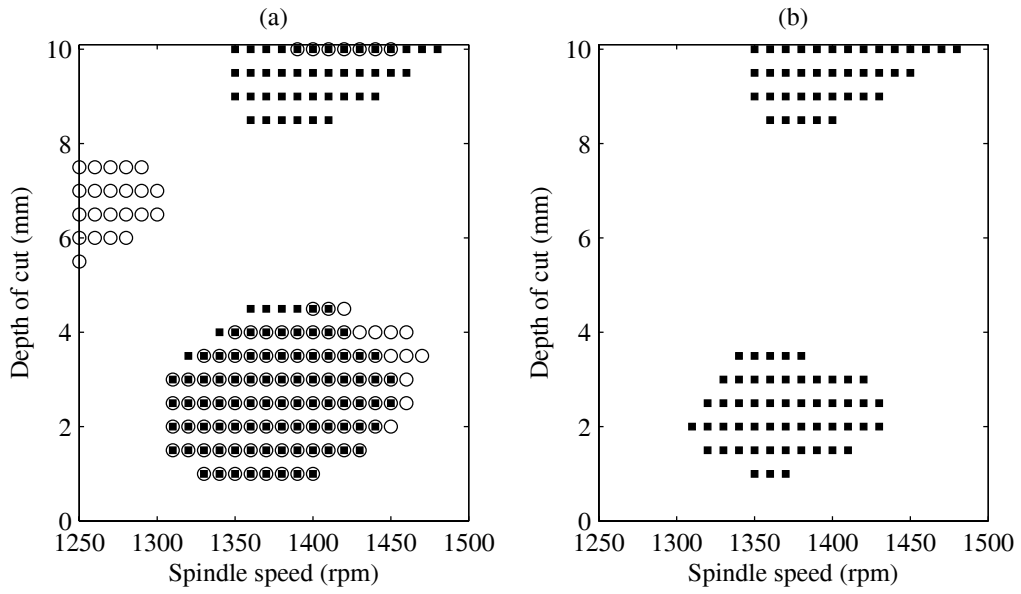


Figure 14: Stability predictions for a two-flute variable helix tool at 100% radial immersion.
(a) analytical methods (b) time domain simulation.
 ■ secondary Hopf bifurcation (semi-discretisation method and time-domain model);
 ○ secondary Hopf bifurcation (time-averaged semi-discretisation method);